

INVESTIGATION OF THE BIAXIAL FRACTURE TOUGHNESS ON CRUCIFORM SPECIMEN CONTAINING HYDROGEN FLAKES

Franck Tankoua¹, Clementine Jacquemoud¹, Minh Bao Le², Guy Roussel³

¹ Research Engineer, Université Paris-Saclay, CEA, Gif-sur-Yvette, France (franck.tankoua@cea.fr)

² Research Engineer, ASNR, Fontenay-aux-Roses, France

³ Research Engineer, BelV, Bruxelles, Belgium

ABSTRACT

This paper focuses on studying the fracture toughness under biaxial loading of a forged ferritic steel containing numerous hydrogen flakes. Ultrasonic control tests were performed to determine the position of hydrogen flakes within the material block. An experimental protocol has been set up so that large cruciform specimens could be tested in five-point bending. These specimens contained a surface fatigue precrack, acting as a fracture initiator, surrounded by multiple tilted hydrogen flakes. The fracture test was performed at -100°C to be close to the reference temperature of the studied material. 3D elasto-plastic finite element calculations have been performed to determine the material fracture toughness for the considered loading configuration.

INTRODUCTION

After about 30 years of operation, the reactor pressure vessels (RPVs) of the Doel 3 and Tihange 2 pressurized water reactors (PWR) in Belgium were found to contain a large number of hydrogen flake defects, mainly concentrated in the circumferential planes of the core shell (or beltline). The hydrogen flakes were associated with zones of segregation of non-metallic inclusions in the low-alloy steel cylindrical forgings used to manufacture the core-shell parts of the RPVs and have been shown to have been generated during forging operations where hydrogen content control was inadequate. Independent of the analytical and experimental efforts carried out in Belgium to justify the serviceability of these RPVs, a test programme was initiated in France by the CEA and the IRSN to verify that the presence of hydrogen flakes was not symptomatic of a weaker material.

The first phase of this test programme (Jacquemoud and Delvallée-Nunio (2018)) included fracture toughness Compact Test (CT) specimens. Nevertheless, the uniaxial loading conditions on CT specimens do not represent the RPV loading conditions. In fact, under either its normal operating conditions or a pressurised thermal shock (due to the safety injection of cooling water), the RPV undergoes biaxial loadings. Therefore, the impact of hydrogen flakes must be assessed in biaxial loading conditions to verify that their presence does not affect the fracture toughness in the plasticity, triaxiality and crack depth conditions representative of a pressurised thermal shock.

In the present study, a five-point bending test was performed on a large cruciform specimen with semi-elliptical cracks (i.e. shallow crack representative of reference defect used in safety assessment) so that both the geometry and loading conditions are representative of RPV. The biaxial fracture toughness was investigated via 3D elasto-plastic finite element calculations, and compared to uniaxial fracture toughness previously assessed with (CT) specimens.

MATERIAL AND SAMPLE PREPARATION

Material

The investigated material is an 18MnD5 ferritic steel containing laminar hydrogen-induced flakes. It was extracted from a steam generator shell, which was discarded at the end of the forging process because of a non-compliance issue. Indeed, to bring evidence to the study case of Doel 3 and Tihange 2 RPV, the material must be similar on various points. First, it contains flakes induced by a similar hydrogen embrittlement phenomenon that had occurred during the shell forging and degassing heat treatment process. Second, it comes from a similar (to the RPV) large forging nuclear equipment. Third, the material in the blocks dedicated to the experiments must be in the same state as the one in the component in operation, which means that the studied material has been submitted to quenching, tempering and equivalent Post Weld heat treatments. The ladle chemical composition of the material is reported in Table 1.

A block containing a high density of flakes was extracted from the top of the steam generator shell. The position and the size of the hydrogen flakes (penny-shaped indication up to 10–15 mm) were determined within the block using ultrasonic inspection. A fine step size of 1 mm was used for acquisition, and the flake shape was approximated to disks or ellipsoids parallel to the top surface of the block. A sketch of all the hydrogen flakes in the volume of the block was designed from the results of ultrasonic analyses, so that specimens could be precisely cut from the block (Figure 1).

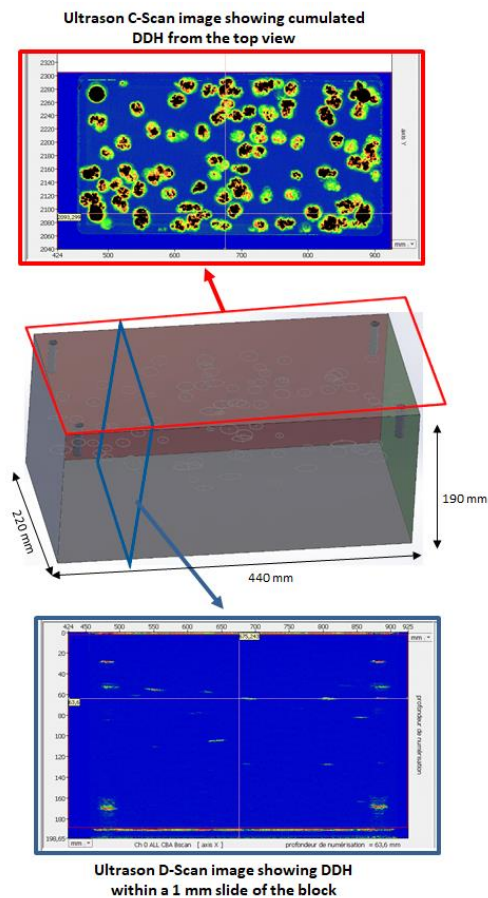


Figure 1. Sketch of the block with numerous hydrogen flakes included. C-Scan and D-Scan images are represented.

Table 1: Ladle chemical composition of the material (wt%).

C	Mn	Si	P	Cr	Mo	Ni	Cu	S	Fe
0.18	1.46	0.17	0.006	0.254	0.5	0.72	0.05	0.002	bal.

Sample preparation

The specimen geometry of this study included a 98 mm thick cruciform core illustrated in Fig. 2a and four extended arms (Fig. 2b), welded on the core to fit the five-point bending rig with a 650 mm distance between supporting plots. A semi-elliptical notch of $a = 10$ mm in depth and $2c = 42$ mm in width was machined at the centre of the specimen. The cruciform core had four series of four machined slots to create a larger zone with uniform biaxial stress in the centre of the specimen where the semi-elliptical notch was located (Lebedev and Muzyka (1998)).

The most critical step for the preparation of the cruciform specimen is the good positioning of the specimen core within the block. A tilting angle of 15° between the crack plane and the surrounding flakes was required for the cruciform specimen to represent the actual loading conditions of Doel-3 and Tihange-2 reactor pressure vessels. To fulfill this requirement, many trials were necessary to find the optimal position of the specimen within the block presented in Figure 3. For this core configuration, an amount of ten flakes surrounded the semi-elliptical notch. The closest flakes were at about 10 mm from the semi-elliptical notch front.

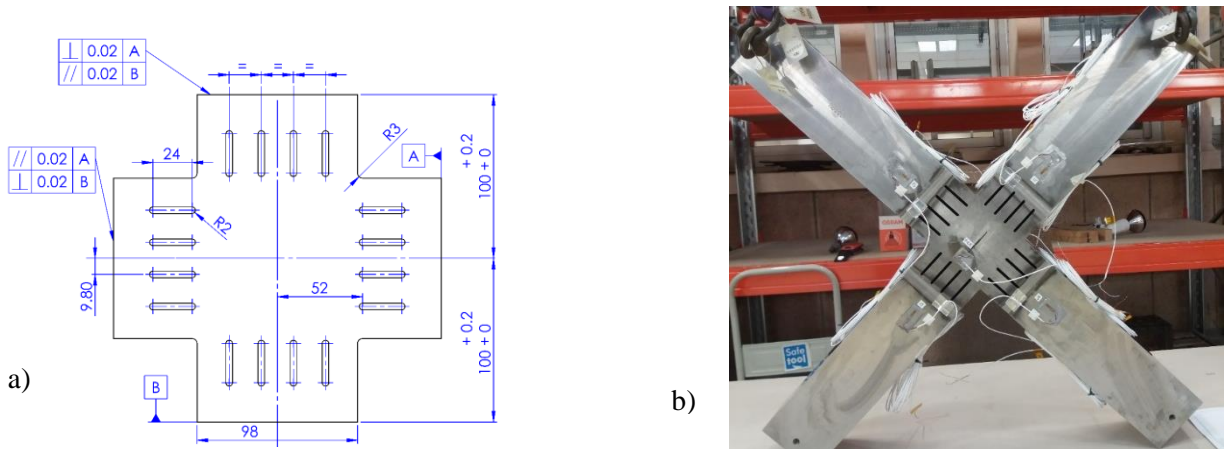


Figure 2. Cruciform specimen with a 98 mm thickness: **a)** core geometry of the specimen, **b)** whole specimen with its arms.

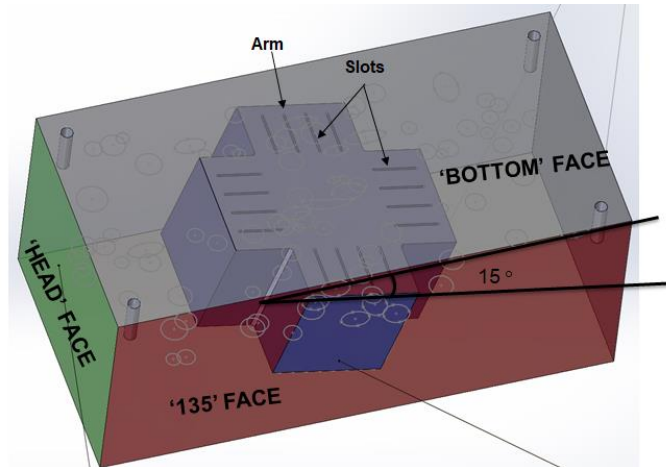


Figure 3. Positioning of the cruciform specimen core within the flaked block – flakes are represented by grey circles

TESTING DEVICE AND PROCEDURE

The biaxial loading tests were performed on a five-point bending rig, inside a climatic chamber on a 2500 kN servohydraulic testing machine (Fig. 4). The specimen balance on the bending rig was validated by sixteen strain gages positioned on the core and the arms.

Prior to the fracture test, a precracking stage was performed to produce a theoretical 2 mm length fatigue crack from the semi-elliptical notch, leading to an a/W ratio of 0.12. The fatigue pre-cracking phase consisted of four steps with decreasing loading level: the initial ΔK_I value (estimated with finite element calculation) was around $25 \text{ MPa}\cdot\text{m}^{0.5}$ and the final one around $15 \text{ MPa}\cdot\text{m}^{0.5}$. During the fatigue precracking, the mean crack depth was estimated via the compliance variation of the specimen, and the surface crack length was monitored by two crack propagation gages.

The fracture tests were conducted at a temperature of -100°C with a prescribed load line displacement rate of 0.002 mm/s . The temperature homogeneity and stability were controlled by three thermocouples welded on the specimen close to the fatigue precrack. The crack mouth opening displacement (CMOD) was measured with a clip gage during the test. The fracture surfaces of the post-mortem specimens were observed using scanning electron microscopy.



Figure 4. Five-point bending rig in the thermal chamber

FINITE ELEMENT MODEL FOR NUMERICAL CALCULATIONS

The tests on cruciform specimens were modelled by using the finite element method on Cast3M software, with implicit integration scheme. Three-dimensional meshes including quadratic, twenty-node elements (47,500 total) were used. Only one-quarter of the specimen was modelled, together with the usual symmetry conditions. The mesh and the boundary conditions applied for the calculation are detailed in Fig. 5. The fatigue crack geometry experimentally measured on the fracture surface was used in the model.

An isotropic yield criterion was used for elastoplastic calculations. The material constitutive parameters were identified from the experimental strain stress curve of the flaked block at -100°C (Figure 6). A Poisson ratio $\nu = 0.3$, and Young modulus = 209 GPa were considered, with an isotropic hardening.

The finite element simulations were used to evaluate the J-integral and the equivalent stress intensity factor (K_J) as no analytical formula was available..

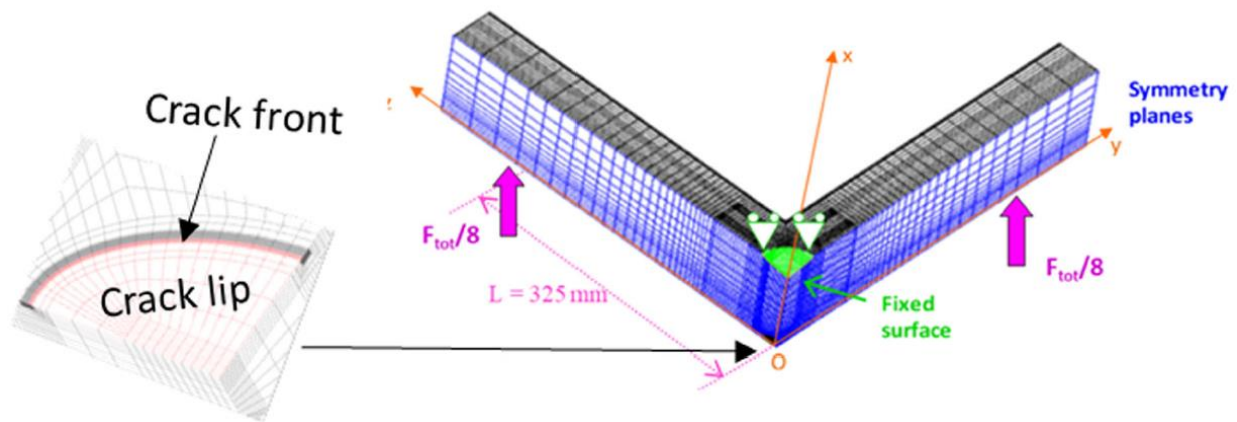


Figure 5. Mesh and boundary conditions used in the FE model

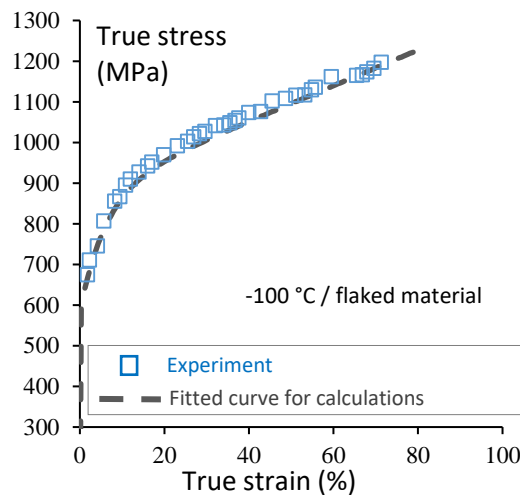


Figure 6. Experimental and simulated strain stress curve used for FE calculations

RESULTS

Load – CMOD curve

The load vs CMOD curve is presented in Fig. 7. At the fracture onset, 1825 kN maximal load was measured. The numerical prediction is in good agreement with the experimental result.

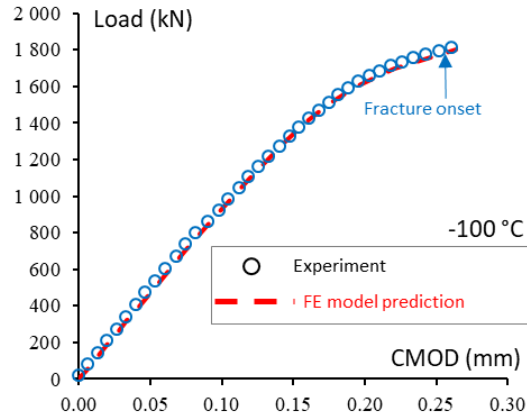


Figure 7. Load vs CMOD curve of the biaxial test at -100 °C in the flaked block. The dashed line is the finite element model prediction

Fracture surface

The fracture surface is presented in Fig. 7a. The brittle crack was initiated from multiple sites on the fatigue precrack. The indications of flakes behind the fatigue crack front validate the good positioning of the specimen. The fatigue crack front is partially covered by a secondary crack initiated from the notch slot (on the left hand side of Fig. 7a).

As presented in Fig. 7b, the experiment fatigue precrack front is slightly deeper than the expected 2 mm propagation.

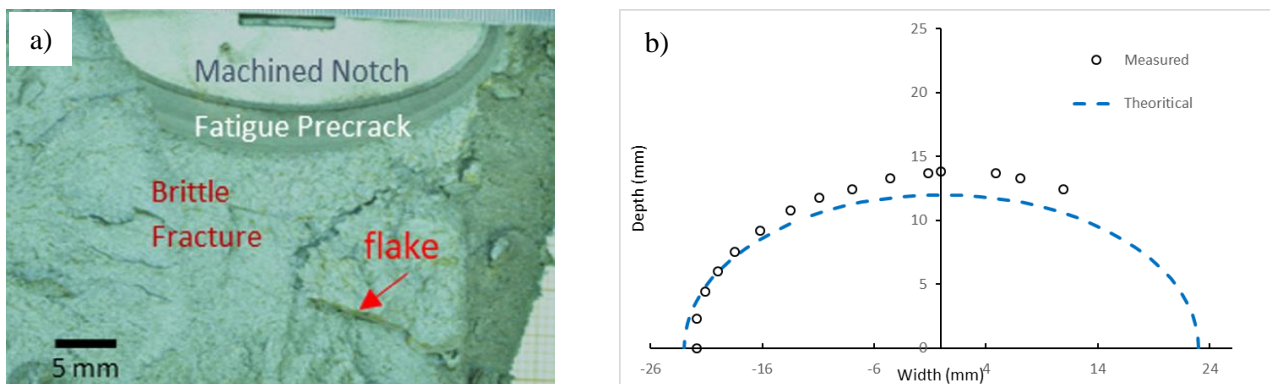


Figure 7. a) Fracture surface of the cruciform specimen, b) Fatigue precrack front.

Biaxial fracture toughness

The stress intensity factor values K_J were estimated using equation (1). The crack length correction was applied with the recommendations of the ASTM E1921 standard. The standard formulation was adapted in equation (2) for the case of a part through-wall elliptical defect, as proposed in Moinereau et al. (2014). The as-measured value of stress intensity factor obtained was $K_{JIT} = 135 \text{ MPa.m}^{0.5}$, and the corrected value was $K_{JIT} = 160 \text{ MPa.m}^{0.5}$.

As presented in Table 2, the fracture toughness in biaxial loading conditions is higher than the uniaxial fracture toughness, even at 99% failure probability.

$$K_J = \sqrt{\frac{J E}{(1-\nu^2)}} \quad (1)$$

$$K_{JIT} = 20 + [K_J - 20] \left(\frac{\text{crack length}}{25} \right)^{1/4} \quad (2)$$

Table 2: Comparison between biaxial fracture toughness and uniaxial fracture toughness on CT.

Biaxial fracture toughness	Uniaxial fracture toughness on CT			
	5% of failure probability	50% of failure probability	95% of failure probability	99% of failure probability
160 MPa.m^{0.5}	60 MPa.m ^{0.5}	100 MPa.m ^{0.5}	130 MPa.m ^{0.5}	150 MPa.m ^{0.5}

CONCLUSION

The effect of hydrogen flakes on fracture toughness was investigated for biaxial loading conditions. The fracture toughness of cruciform specimens is considerably higher than the fracture toughness of CT specimens at -100 °C. The positive effect of a lower constraint level combined with a shallow crack (larger plasticity) is confirmed. The presence of multiple flakes ahead of the fatigue precrack, at a minimum distance of 10 mm, does not cancel the positive effect. This confirms the conservatism of the fracture analysis based on standard CT specimens. Additional tests in biaxial loading conditions may be required on the flaked material to confirm the positive effect observed on fracture toughness.

ACKNOWLEDGMENTS

IRSN (ASNR) and CEA are thankful to M. Claude BENHAMOU and M. Pierre JOLY from Framatome who provided the material of the study and expertise that assisted the research. They are also grateful to BEL V for its financial support in the second phase of the test programme. CEA-LIST involvement in the ultrasonic examinations is gratefully acknowledged.

REFERENCES

“ASTM standard test methods for determination of reference temperature, t_0 , for ferritic steels in the transition range”, *ASTM E1921 Standard, American Society for Testing of Materials*, West Conshohocken, PA. <https://doi.org/10.1520/E1921-23>

Jacquemoud, C., Delvallée-Nunio I. (2018) “Mechanical behaviour of a forged ferritic steel shell containing numerous hydrogen flakes,” *Pressure Vessels and Piping Conference*, July 2018, Prague, Czech Republic, ISBN: 978-079185158-6, Vol. 1A, <https://doi.org/10.1115/PVP201884087>

Lebedev, A.A., Muzyka, N.R. (1998) “Design of cruciform specimens for fracture toughness tests in biaxial tension (Review),” *Strength Mater* 30:243-254. <https://doi.org/10.1007/BF02524723>

Moinereau, D., Chapuliot, S., Marie, S., Jacquemoud, C. (2014) “NESC VII synthesis: A European project for application of WPS in RPV assessment including biaxial loading,” *Pressure Vessels and Piping Conference*, July 2014, Anaheim, United States of America, ISBN: 978-079184603-2, Vol. 6A, <https://doi.org/10.1115/PVP2014-28076>